

Initializing anisotropic and unstable electron velocity distributions needed for investigating plasma kinetic instabilities

C.-K. Huang, C.-J. Zhang, K. A. Marsh, C. E. Clayton, and C. Joshi

University of California Los Angeles Department of Electrical Engineering, Los Angeles, California 90095, USA

(Dated: April 23, 2019)

Plasmas with anisotropic electron velocity distribution functions are needed for the controlled study of kinetic plasma instabilities in the laboratory. We demonstrate that such plasma can be produced using ultrashort laser pulses via optical-field ionization (OFI). We experimentally show this control by using Thomson scattering as a diagnostic to probe the characteristic electron velocity distributions using linearly and circularly polarized laser pulses to ionize helium. Furthermore the He plasma produced by a circularly polarized light pulse exhibits the onset of the electron streaming instability within 300 fs of ionization, demonstrating applicability of OFI generated plasmas for studying the kinetic theory regime of plasma physics.

The theoretical foundation of plasma physics has a conceptual hierarchy: exact microscopic or single particle description, kinetic theory and fluid theory [1]. There are important physical problems where the complete microscopic description is impractical while the fluid model is inadequate. In such cases the plasma is described in terms of one or more velocity distribution functions—this is the basis of kinetic theory of plasmas [2]. Experimental verification of these kinetic effects is predicated upon the ability to control or know the velocity distribution functions of the plasma species. For instance temporal evolution of kinetic phenomena such as plasma wave generation by inverse Landau damping [3] and instabilities such as the streaming [4], electron filamentation [5] and Weibel [6] could be quantitatively compared with theory if suitable electron velocity distribution functions (EVDF) could be initialized in a plasma. Aside from their fundamental interest, these kinetic effects are encountered in space plasmas [7], fast ignition fusion [8], high-energy colliders [9], neutrino-plasma interactions [10] and recombination X-ray lasers [11]. With the advent of femtosecond lasers it has become possible to manipulate the EVDF by optical field ionization (OFI) of atoms or molecules. Specifically by using an appropriate combination of laser wavelength(s), intensity profile, polarization, direction of propagation and ionization state of gases/molecules one can create plasmas with known EVDF. In this article, we experimentally demonstrate two examples of such nonthermal and anisotropic distribution functions by ionizing both electrons of He using fs-class linearly and circularly polarized laser pulses and show evidence for the electron streaming instability within 300 fs after the formation of the plasma.

Optical-field ionization of gases becomes dominant over multi-photon ionization when the Keldysh parameter is in the tunnel ionization regime, i.e. $\gamma = (U_i/2U_p)^{1/2} \ll 1$ where U_i is the ionization potential and U_p is the ponderomotive potential of the laser [12]. The energy and the direction of the ionized electron in OFI depends upon the details of the laser pulse(s) and the ionization state of the gas [13–16]. In Fig. 1 we show four examples. Generally speaking the electrons are ejected

transverse to the wave vector of the laser pulse along the direction of its polarization in the non-relativistic limit ($a_0 \leq 1$), producing strongly non-thermal and/or anisotropic EVDF in the resulting plasma. Here $a_0 = eA/mc^2 = eE/m\omega c$ is the normalized laser strength parameter, where A is the vector potential, E is the laser electric field, and ω is the laser frequency. The EVDF of highly charged states produced by relativistic pulses ($a_0 \geq 1$) in a dense plasma are rather complicated because they can be affected by numerous other physical effects such as wakefields/parametric instabilities [17, 18], direct energy exchange with the laser field [19] and therefore will not be considered here. The polarization dependence of OFI produced electrons has been tested in previous work in either the long-wavelength [13] or the barrier suppression limit using very low-pressure gases [20, 21]. Leemans et al. [22] showed that it was possible to control the Raman instability by varying the polarization of a 200 ps CO₂ laser produced OFI plasma. Moore et al. [23] showed that when intense ($a_0 \sim O(1)$), longer laser pulses are used, the electrons gain additional energy from the ponderomotive potential of the laser envelope. Glover et al. [24] used Thomson scattering diagnostic to fit the scattered light spectrum from an OFI He plasma produced using a linearly polarized 800 nm pulse but they did not observe scattering from each of the two ionic species of He. Thus, no experimental confirmation of the nonthermal and/or highly anisotropic initial EVDF characteristic of OFI plasmas has been made to-date even though the kinetic instabilities that follow the creation of such plasmas have been predicted [25–27].

In Fig. 1 we show four examples of such EVDF in velocity space (v_x vs v_y) using the 3D particle-in-cell (PIC) code OSIRIS [28] where the formation of a fully ionized, dense ($5 \times 10^{18} \text{ cm}^{-3}$) He plasma is modeled using the ADK theory [29]. In all cases the simulations consider tunnel ionization of electrons [12] ($\gamma_{\text{He}^{1+}} = 0.38$ and $\gamma_{\text{He}^{2+}} = 0.23$) and self-consistently include other physical effects such as the ponderomotive force of the optical pulse, plasma kinetic effects, and wake formation. We shall refer to the electron that ionizes first as the He¹⁺ electron and second as the He²⁺ electron. The EVDF

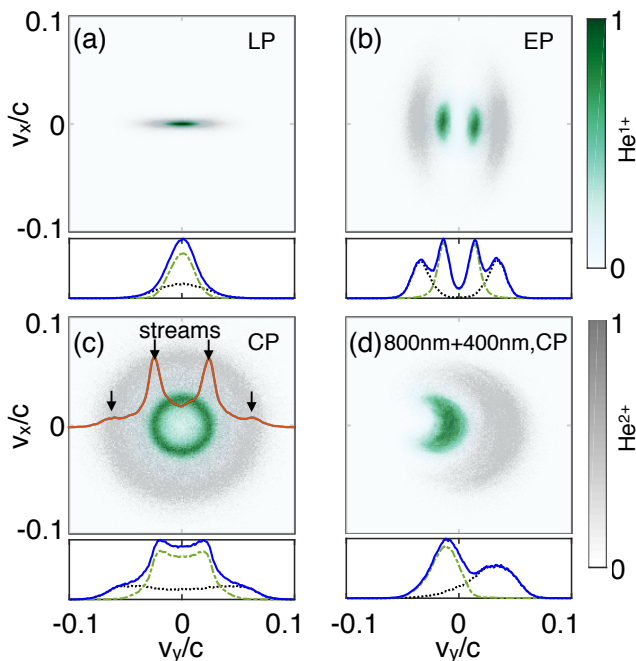


FIG. 1. (a)-(c) Examples of simulated electron velocity distributions using OSIRIS of He plasmas produced by 50-fs, 800 nm laser pulses with peak intensity of 1.6×10^{17} W/cm² and different polarizations (linear, elliptical, circular respectively). (d) circular, 800 nm, 3×10^{16} W/cm² + circular, 400 nm, 1×10^{16} W/cm² with the same initial phase. The red curve in (c) shows the lineout at $v_x = 0$ showing four streams. Also shown below each $v_x - v_y$ image is the v_y distribution (the sum of the number of particles at each v_y) for He¹⁺ electrons (dashed green curve), He²⁺ electrons (dotted black curve) and their sum (solid blue line).

shown here are just after the passage of the laser pulse. Here the x-y plane is perpendicular to the direction of propagation of the laser, z. In these cases the He¹⁺ electrons are ionized early during the risetime of the laser pulse within a few laser cycles and the He²⁺ electrons are ionized approximately 10 fs after the first He electron. These electrons have both transverse (x and y) and longitudinal (z) oscillating energy of a few eV due to a weak linear wake formed by the laser pulse [17] and the ions are essentially cold in all directions. We manipulate the EVDF in Fig. 1 by changing the polarization of the laser pulse to ionize He atoms from linear (a), to elliptical (b) to circular (c, d). Figure 1(a) shows that the initial electron distribution along the laser polarization direction (y) in the linear polarization (LP) case can be well described by a sum of two 1D (near) Maxwellian distributions with temperatures of 60 eV (He¹⁺) and 210 eV (He²⁺) respectively. In the elliptical polarization case (degree of ellipticity $\alpha = 0.5$, (Fig. 1(b)) the EVDF shows four lobes with the distribution in x much wider than that in y. Once again the He²⁺ electrons (gray) are more energetic than He¹⁺ electrons. In the circular polarization (CP) case (Fig. 1(c)), electron distributions

are donut-shaped in the x-y velocity space. In the x-y plane the resulting electron velocity distribution has 4 radial streams. The transverse streams in Fig. 1(b) and the radial streams in Fig. 1(c) have larger drift velocities than their thermal velocities. Kinetic theory predicts that plasmas with such distribution functions are susceptible to developing kinetic instabilities [2]. It is the relative drift between these streams that gives rise to the electron streaming instability. The existence of electrons close to zero transverse velocity suggests that the plasma has already evolved by the end of the laser pulse, due to collective effects. The overall initial electron distribution in the circular case is also shown in Fig. 1(c), blue curve. It indicates a highly non-Maxwellian distribution with much hotter root-mean-square (rms) temperature of ~ 470 eV (220 eV and 910 eV for the He¹⁺ and the He²⁺ electrons respectively). In case 1(d) a two frequency CP laser pulse with different intensities generates a bump-on-tail distribution that would lead to spontaneous generation of plasma waves via inverse Landau damping. From the above examples, it is clear that numerous other “designer” EVDFs are possible by optimization of laser and choice of the ionizing medium.

As mentioned earlier the measurement of the EVDF is difficult because plasmas can very quickly develop kinetic instabilities. These collisionless processes tend to isotropize the initially produced EVDF on a timescale far shorter than electron-electron collisions alone, estimated to be tens of ps for typical value of $T_{x,y}/T_z$ expected here. We therefore use the Thomson scattering diagnostic with ~ 90 fs (FWHM) probe pulses to interrogate the EVDF of the OFI helium plasma just ~ 300 fs after ionization is completed. During such a short time period plasma density evolution due to expansion or recombination can be neglected.

The experimental setup is shown schematically in Fig. 2. The plasma was formed by ionizing a static fill of He gas at various pressures by focusing a 800 nm, ~ 50 fs (FWHM) duration laser pulse containing ~ 10 mJ energy. The laser was focused by an off-axis parabolic mirror (OAP) to a spot size $2w_0$ of $16 \mu\text{m}$ giving a peak intensity of $\sim 1 \times 10^{17}$ W/cm². The ~ 1 mJ, ~ 90 fs (FWHM), 400 nm probe pulse is generated by a 1.5-mm-thick KDP crystal. The total group delay (τ_g) between the pump and the probe is estimated to be ~ 300 fs. The probe beam was focused by the same OAP and focused to a even smaller spot size within the fully ionized plasma. Thomson scattered light was collected at 60° with respect to (w.r.t.) the incident pulse by a one-to-one imaging system that relays image of the central part of the plasma to the entrance slit of the spectrograph. The plane containing the incident probe wave vector (\vec{k}_{pr}) and the scattered light wave vector (\vec{k}_s) is referred to as the scattering plane. Two polarization configurations for linearly (L) polarized pump beams are the polarization direction parallel (L_{\parallel}) or perpendicular (L_{\perp}) to the scattering plane. The L_{\parallel} (L_{\perp}) polarization allows us to independently probe the EVDF essentially along the v_y

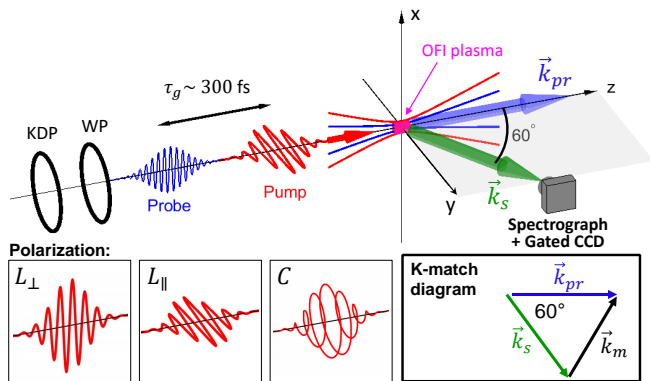


FIG. 2. Schematic of the experiment. The 800 nm pump beam generates OFI plasmas that are probed by a collinear 400 nm Thomson scattering beam using a fixed delay: linear polarization perpendicular to the scattering plane (L_{\perp}), parallel to the scattering plane (L_{\parallel}) and circular polarization (C). Also shown is the k-matching diagram where the vector \vec{k}_m is probed in Thomson scattering. KDP: KDP crystal; WP: half-wave plate for linear polarization or quarter-wave plate for circular polarization.

(v_x) directions as shown in Fig. 1(a). There is only one configuration for circular polarization (C) since the “double donut” EVDF generated is transversely isotropic (Fig. 1(c)).

The measured scattered spectra are used to infer the near instantaneous status of OFI plasmas by comparing them with the Thomson scattering theory [30]. All the data shown in this paper are the average of 200 consecutive shots to improve the signal-to-noise ratio. For a non-relativistic, non-magnetized plasma with an electron distribution function $f_e(\vec{v})$ and an ion distribution function $f_i(\vec{v})$, Thomson scattering spectral power density (SPD) function can be written as

$$S(\vec{k}, \omega) = \frac{2\pi}{k} \left| 1 - \frac{\chi_e}{\epsilon} \right|^2 f_e\left(\frac{\omega}{k}\right) + \frac{2\pi Z}{k} \left| \frac{\chi_e}{\epsilon} \right|^2 f_i\left(\frac{\omega}{k}\right) \quad (1)$$

where Z is the atomic number of the atom, $\epsilon = 1 + \chi_e + \chi_i$ is the dielectric function, χ_e and χ_i are the electron and ion susceptibilities. We can apply arbitrary distribution functions f_e and f_i to calculate $S(\vec{k}, \omega)$ and get the spectral shape of the Thomson scattered light. Due to the broad bandwidth of the probe beam (~ 3.4 nm) and the limiting wavelength resolution (~ 1 nm) of the spectrograph, the ion feature spectrum is not resolved in our experiment and thus information about the plasma comes from the first term in Eq. (1). The 60° scattering angle determines the measured \vec{k}_m in this experiment as depicted in Fig. 2. It should be noted that the temperatures of the two-Maxwellian distributions in the experiments are expected to be different than those from the simulations since we observe the plasma along \vec{k}_m which has a 30° angle with respect to the transverse plane used

in simulations. The observable temperatures, which are evaluated from the projection of the distribution onto the measured wavevector [31], are about 45 and 160 eV for polarization L_{\parallel} .

The scattered light spectra from plasmas produced by LP pump taken at two fill pressures are shown in Fig. 3. The central spectral feature at around 400 nm is the ion feature which is not frequency resolved in this experiment. The frequency shift of the “electron feature”, which is associated with collective scattering from electron plasma waves is symmetric on either side of the ion feature. The red dashed line in each plot is the best fit of the calculated SPD function $S(\omega)$. Figure 3(a) and 3(b) show the spectra where the polarization is perpendicular to the scattering plane (L_{\perp}). We found that a single Maxwellian distribution with electron temperature of 18 ± 2 eV (room temperature ions) fits spectra obtained at both low (10 torr) and high (75 torr) pressures. The corresponding temperature in the perpendicular plane after 300 fs is expected to be ~ 12 eV from simulations. Thus there is a reasonable agreement between the experiment and the simulations.

The scattering spectra when the linear polarization is in the scattering plane L_{\parallel} are shown in Fig. 3(c) and 3(d) also for helium fill pressures of 10 and 75 torr respectively. In this case, the calculated SPD functions given by a single Maxwellian distribution (not shown) do not fit with the experimental spectra. The data were therefore fitted by taking a two-temperature distribution into consider-

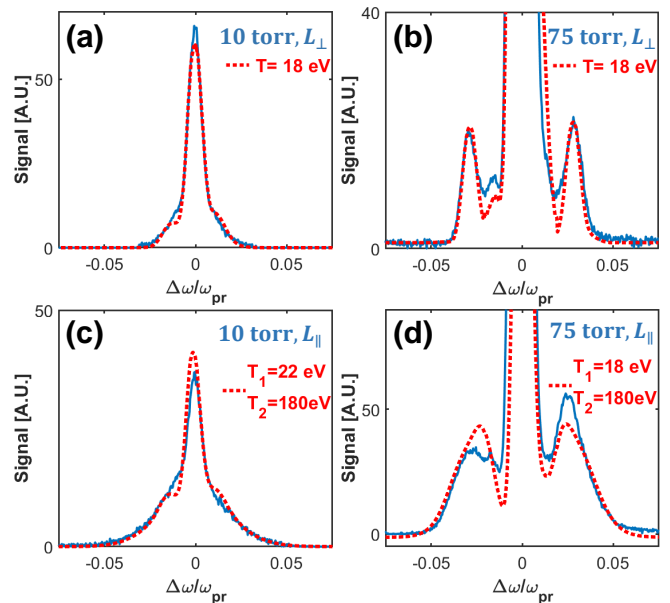


FIG. 3. Thomson scattering spectra for linear polarization (blue curves- experimental spectra; dotted red curves- calculated spectra). Polarization direction is out of the scattering plane for (a) and (b) and parallel to the scattering plane for (c) and (d). The L_{\perp} cases can be fit by a single temperature of 18 eV whereas the L_{\parallel} cases require a two-temperature fit as shown.

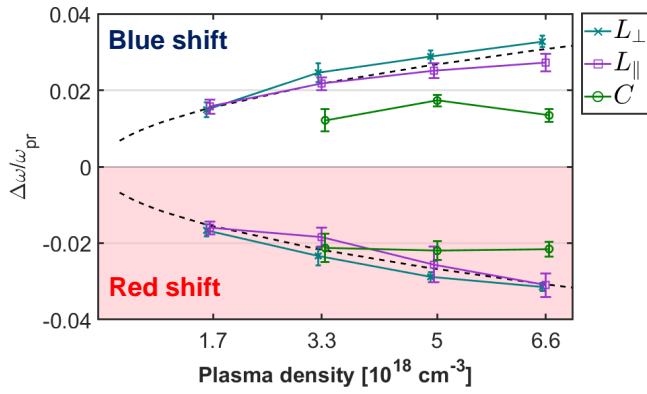


FIG. 4. The measured spectral peak shifts of the electron feature for different plasma densities and different laser polarization (L_{\perp} , L_{\parallel} , C). The error bars show the standard deviation of the shifts for 100 shots. The plasma densities plotted correspond to fully ionized He at 25, 50, 75, and 100 torr. The dashed lines show the variation of frequency shift equal to the plasma frequency, $\Delta\omega = \omega_{pe}(n_e)$.

ation. Substituting $f_e = 0.5f_{e,T_1} + 0.5f_{e,T_2}$ into Eq. (1) where T_1 and T_2 are fitting parameters ($T_2 > T_1$) while keeping the ions as a fixed ultra-cold component, we get a new set of SPD functions that describe the scattering spectra for the linear polarization case. The best fits give $T_1 = 20 \pm 2$ eV and $T_2 = 180 \pm 20$ eV. The agreement here with the simulations is again reasonable. We can see that the theoretical plots shown Fig. 3(c) and 3(d) fit less well than those for Fig 3(a) and 3(b) both taken at the same pressure but in the orthogonal plane.

The frequency shift of the electron feature in the collective scattering regime should increase as the Langmuir wave frequency, ω_{pe} . Figure 4 shows the measured spectral peak shifts for various plasma densities for different polarization configurations. For both L_{\perp} and L_{\parallel} , the shifts of their sideband peaks both increase with densities as expected. This is clearly not the case in the case of circular polarization which is also shown. The frequency shift of the electron feature for the CP case was almost independent of the plasma density, which is indicative of some other collective phenomena being dominant collective scattering mechanism than the usual Langmuir waves.

The Thomson scattered spectra for the CP pump pulses are shown in Fig. 5. Recall that the electrons in this case have higher average kinetic energy than those with LP and the EVDF deviate greatly from Maxwellian. Our fitting attempt using Eq. (1) failed with either one-temperature or two-temperature Maxwellian distributions as expected. At low enough plasma densities collective effects are not important and one expects photons to be Doppler up or down shifted because of the individual electron motion irrespective of the shape of the EVDF. We found that it is possible to fit the experimental spectrum taken at this low plasma density using the distribution function observed in the simula-

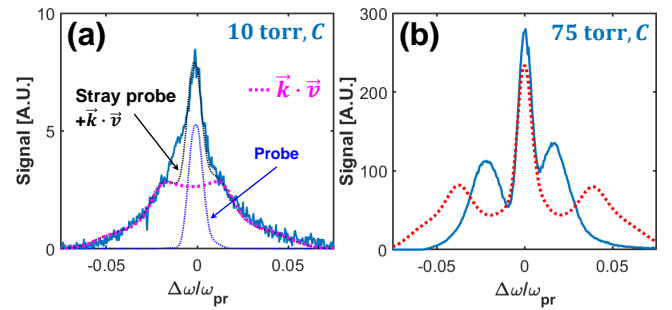


FIG. 5. Thomson scattering spectra for circular polarization averaged over 200 shots: (a) The measured spectrum at 10 torr He pressure and a fit that is the sum of the Doppler shifted spectrum (dotted pink curve) expected from the electron distribution shown in Fig. 1(c) and stray light spectrum of the probe beam (dotted blue curve). (b) The measured Thomson scattered spectrum at 75 torr (blue curve) and the calculated spectrum (dotted red curve) using a distribution with two pairs of drifting Maxwellian counter streams (drift velocities of $\pm 0.015c$ and $\pm 0.046c$, widths of 87 and 79 eV, and a density ratio of $\sim 4 : 1$) deduced from the EVDF shown in Fig. 1(c).

tion as shown in Fig. 1(c). The simulated EVDF fits to the wings of the total spectrum with a plasma density of $6.6 \times 10^{17} \text{ cm}^{-3}$ used in the experiment. When the spectrum of the stray probe photons is also taken into account the overall Doppler shifted plus the stray photon spectrum fits the experimentally measured spectrum extremely well. This excellent fit confirms that the EVDF in the CP case has four streams in the radial direction as shown by the lineout in Fig. 1(c). For the higher density case (Fig. 5(b)) two distinct spectral “electron” peaks with asymmetric shifts appeared. Their frequency shifts were both $\leq \omega_{pe}$ and independent of the plasma density as was not the case with LP shown in Fig. 4. This is expected if the scattering is from the streaming instability where the spectral shift depends on the streams’ drift velocity, $\Delta\omega \sim k_m \cdot v_d$ where v_d is the relative drift velocity between electron streams which is independent of plasma density. Substituting the observed spectral shift of two satellites we obtain $|v_d|$ equal to $(0.02 \pm 0.002)c$ (blue) and $(0.025 \pm 0.005)c$ (red) respectively. Since $k_m = k_r + k_z$ we are actually observing the oblique electron streaming instability. This is confirmed in the OSIRIS simulations. The streaming instability onset occurs in the the x-y plane as expected but it quickly spreads in all three dimensions this in turn leads to the onset of the electron streaming instability in an oblique direction [32] that we observe here. This is the first laboratory observation of the electron streaming instability because of the anisotropy of the EVDF of the plasma electrons to our knowledge. The reason why one can measure the density dependence of the plasma frequency using Thomson scattering in the LP case is that the onset of the two-stream instability happens almost 1 ps later when LP is used compared to when CP laser pulse is

used. This is because the ionization process itself produces relative electron streaming in the CP case whereas the fastest He^{2+} electrons have to bounce off the plasma sheath to begin streaming in LP case [33].

In conclusion, we have demonstrated that OFI may be a method for controlling the initial EVDF in plasmas. We have used Thomson scattering diagnostic to probe two such EVDF within 300 fs of their initialization by OFI in He plasmas using different polarization

configurations. The scattered light spectra are consistent with the expected anisotropic distributions. Until they are isotropized and thermalized such plasmas cannot be described by the fluid theory and thus present a new platform for studying kinetic effects and instabilities in laboratory plasmas.

We thank W.B. Mori for useful discussions. This work was supported by DOE grant [de-sc0010064](#), NSF grant 1734315, AFOSR grant FA9550-16-1-0139 and ONR MURI award N00014-17-1-2705.

-
- [1] F. F. Chen, *Introduction to Plasma Physics and Controlled Fusion*, 3rd ed. (Springer, New York, 2016).
- [2] R. C. Davidson, in *Handbook of Plasma Physics*, Vol. 1, edited by A. A. Galeev and R. N. Sudan (North-Holland, Amsterdam, 1983) p. 229.
- [3] R. Goldston and P. Rutherford, “Introduction to plasma physics,” (CRC Press, Boca Raton, 1995) Chap. 25, p. 429, 1st ed.
- [4] T. H. Stix, *Waves in Plasmas*, 1st ed. (AIP-Press, New York, 1992).
- [5] B. D. Fried, *Phys. Fluids* **2**, 337 (1959).
- [6] E. S. Weibel, *Phys. Rev. Lett.* **2**, 83 (1959).
- [7] R. A. Treumann and W. Baumjohann, *Advanced Space Plasma Physics* (Imperial College Press, London, 1997).
- [8] J. T. Mendonca, P. Norreys, R. Bingham, and J. R. Davies, *Phys. Rev. Lett.* **94**, 245002 (2005).
- [9] K. Ohmi and F. Zimmermann, *Phys. Rev. Lett.* **85**, 3821 (2000).
- [10] R. Bingham, H. Bethe, J. Dawson, P. Shukla, and J. Su, *Phys. Lett. A* **220**, 107 (1996).
- [11] N. H. Burnett and G. D. Enright, *IEEE J. Quantum Electron.* **26**, 1797 (1990).
- [12] L. V. Keldysh, *J. Exp. Theor. Phys.* **20**, 1307 (1965).
- [13] P. B. Corkum, N. H. Burnett, and F. Brunel, *Phys. Rev. Lett.* **62**, 1259 (1989).
- [14] L. Zhang, X. Xie, S. Roither, D. Kartashov, Y. L. Wang, C. L. Wang, M. Schöffler, D. Shafir, P. B. Corkum, A. Baltuška, I. Ivanov, A. Kheifets, X. J. Liu, A. Staudte, and M. Kitzler, *Phys. Rev. A* **90**, 061401 (2014).
- [15] D. Dimitrovski, J. Maurer, H. Stapelfeldt, and L. B. Madsen, *Phys. Rev. Lett.* **113**, 103005 (2014).
- [16] C. A. Mancuso, D. D. Hickstein, P. Grychtol, R. Knut, O. Kfir, X.-M. Tong, F. Dollar, D. Zusin, M. Gopalakrishnan, C. Gentry, E. Turgut, J. L. Ellis, M.-C. Chen, A. Fleischer, O. Cohen, H. C. Kapteyn, and M. M. Murnane, *Phys. Rev. A* **91**, 031402 (2015).
- [17] C. Joshi, *Sci. Am.* **294**, 40 (2006).
- [18] C. Joshi, T. Tajima, J. M. Dawson, H. A. Baldis, and N. A. Ebrahim, *Phys. Rev. Lett.* **47**, 1285 (1981).
- [19] J. L. Shaw, N. Lemos, L. D. Amorim, N. Vafaei-Najafabadi, K. A. Marsh, F. S. Tsung, W. B. Mori, and C. Joshi, *Phys. Rev. Lett.* **118**, 064801 (2017).
- [20] U. Mohideen, M. H. Sher, H. W. K. Tom, G. D. Amiller, O. R. Wood, R. R. Freeman, J. Bokor, and P. H. Bucksbaum, *Phys. Rev. Lett.* **71**, 509 (1993).
- [21] S. J. McNaught, J. P. Knauer, and D. D. Meyerhofer, *Phys. Rev. Lett.* **78**, 626 (1997).
- [22] W. P. Leemans, C. E. Clayton, W. B. Mori, K. A. Marsh, A. Dyson, and C. Joshi, *Phys. Rev. Lett.* **68**, 321 (1992).
- [23] C. I. Moore, A. Ting, S. J. McNaught, J. Qiu, H. R. Burris, and P. Sprangle, *Phys. Rev. Lett.* **82**, 1688 (1999).
- [24] T. E. Glover, T. D. Donnelly, E. A. Lipman, A. Sullivan, and R. W. Falcone, *Phys. Rev. Lett.* **73**, 78 (1994).
- [25] V. P. Krainov, *J. Exp. Theor. Phys.* **96**, 430 (2003).
- [26] V. Y. Bychenkov, D. V. Romanov, W. Rozmus, C. E. Capjack, and R. Fedosejevs, *Phys. Plasmas* **13**, 013101 (2006).
- [27] K. Y. Vagin and S. A. Uryupin, *Phys. Plasmas* **24**, 103118 (2017).
- [28] R. A. Fonseca, L. O. Silva, F. S. Tsung, V. K. Decyk, W. Lu, C. Ren, W. B. Mori, S. Deng, S. Lee, T. Katsouleas, and J. C. Adam, in *Lect. Notes Comput. Sci.* (2002) pp. 342–351.
- [29] M. V. Ammosov, N. B. Delone, and V. P. Krainov, *J. Exp. Theor. Phys.* **64**, 1191 (1986).
- [30] D. H. Froula, S. H. Glenzer, N. C. Luhmann, and J. Sheffield, in *Plasma Scattering of Electromagnetic Radiation* (Academic Press, Cambridge, 2011) 2nd ed., Chap. 3, pp. 45–68.
- [31] M. V. Chegotov, *Plasma Phys. Rep.* **26**, 602 (2000).
- [32] A. Bret, M.-C. Firpo, and C. Deutsch, *Phys. Rev. E* **70**, 046401 (2004).
- [33] C.-J. Zhang, C.-K. Huang, K. A. Marsh, C. E. Clayton, W. B. Mori, and C. Joshi, (unpublished).